Article

JOURNAL OF COMPOSITE MATERIALS

Journal of Composite Materials
0(0) 1–11

DOI: 10.1177/0021998315573286
jcm.sagepub.com
SAGE

Compressive failure analysis of quasi-isotropic composite laminates fabricated with quasi-unidirectional woven fabric

Bo Wang, Kento Maekawa, Nobuhide Uda, Kousei Ono and Hiroto Nagai

Abstract

The effect of configuration of quasi-unidirectional woven fabric on the compressive failure modes of quasi-isotropic composite laminates was investigated in this study. Two kinds of out-of-plane fiber waviness were formed in the composite laminates due to different quasi-unidirectional woven fabrics and measured using a fast Fourier transform method. The compressive failure modes of the composite laminates were identified using experimental and numerical methods. It was found that the compressive strength of a composite laminate fabricated using long-pitch weft fabrics was greater than that fabricated using standard-pitch weft fabrics. The relationship between the compressive strength and the configuration of quasi-unidirectional woven fabrics was investigated in a parametrical study, and four compressive failure modes were found: the axial compressive, normal, bending, and shear failure modes.

Keywords

Quasi-unidirectional woven fabric, fiber waviness, compressive strength, finite element analysis, vacuum-assisted resin transfer molding

Introduction

Composites are widely used in aerospace, automobile, and many other green energy projects. Therefore, it is necessary to understand the compressive failure modes of composites in a broad range of applications.

The quasi-unidirectional (UD) woven fabric, as an application of composites, is a special woven fabric with unbalanced textile, which is fabricated with around 98% warp and a few weft yarns, as shown in Figure 1. The warp yarns provided a loading capability after consolidation and the weft yarns made the fabric integrity for handling. Unfortunately, fiber misalignment was caused by this textile, which has a negative effect on the compressive properties of the composites.

In 1965, Rosen evaluated the compressive strengths of fiber composites using the theory of elastic stability.[1] He divided the failure modes into an extension mode and a shear mode, and calculated the compressive strength related to the shear mode using equation (1). Unfortunately, this strength was three times larger than the experimental results[2]

$$\sigma_c = \frac{G_m}{V_f} \tag{1}$$

where σ_c is the compressive strength, V_f is the fiber volume fraction, and G_m is the matrix shear modulus.

An initial fiber misalignment was pointed out by Argon in 1972,[3] which sharply decreased the compressive strength as a kind of manufacturing defect. A local shear stress was developed by compressive loading as a result of the fiber misalignment, and led to the instability of the composite. Therefore, the compressive strength was calculated as follows

$$\sigma_c = \frac{\sigma_{12}}{\theta_0} \tag{2}$$

where σ_{12} is the yield shear stress of the composite, and θ_0 is the initial fiber misalignment angle. Subsequently, Budiansky[4] extended the analysis of Argon in an elastic–plastic shear model in 1983, and a shear strain γ

Department of Aeronautics and Astronautics, Faculty of Engineering, Kyushu University, Fukuoka, Japan

Corresponding author:
Bo Wang, Department of Aeronautics and Astronautics, Kyushu University, 744 Motooka, Nishi-ku, Fukuoka 8190395, Japan.
Email: wangbo_8611@hotmail.com

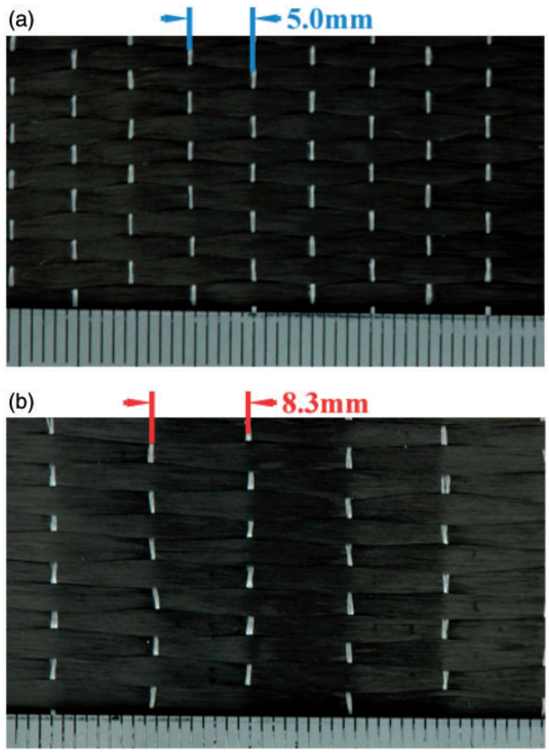

Figure 1. Quasi-UD woven carbon fabrics. (a) standard pitch and (b) long pitch.

corresponding to the local shear stress was included as follows

$$\sigma_c = \frac{\sigma_{12}}{(\theta_0 + \gamma)} \tag{3}$$

However, only averaged fiber misalignment angle was considered in the equation (3), and fiber curvatures are neglected in micro-mechanical model.

The fiber misalignment in laminates, including the in-plane and out-of-plane fiber waviness, has also attracted the attention of researchers. Shuart[5] studied the relationship between the layer orientation and dominant compressive failure modes in laminates containing fiber waviness, and found three failure modes: inter-laminar shearing, in-plane matrix shearing, and matrix compression. Hsiao and his co-workers[6] proposed a new curing method for UD and cross-ply composite laminates with controlled fiber waviness, and studied the elastic properties and failure modes of laminates with uniform, graded, and localized fiber waviness in experimental and theoretical studies.[7,8] They found that the major Young's modulus E_x and compressive strength rapidly decreased as the fiber waviness increased, and the dominant failure mechanism was inter-laminar shearing under axial compression in UD wavy composite laminates. However, the study of the effect of out-of-plane fiber waviness in the quasi-isotropic composite laminates on compressive failures is not profuse.

This paper presents an investigation of the effect of configuration of quasi-UD woven fabric on the compressive failure modes of quasi-isotropic composite laminates. Two kinds of out-of-plane fiber waviness were formed in the composite laminates due to different quasi-UD woven fabrics, and the wavelengths and amplitudes were measured using the fast Fourier transform (FFT) method. The compressive strengths were found in compressive tests, and the effect of the waviness configuration was analyzed in numerical investigation. Finally, the relationship between the compressive strengths and fiber configurations was mapped, and four failure modes were classified in a parametrical study.

Materials

The composite laminates investigated in this study were composed of carbon/epoxy composites. Two kinds of quasi-UD woven fabrics (as shown in Figure 1) were supplied by Mitsubishi Rayon Co., Ltd., which consisted of MR50S 12K carbon fiber warp and a glass fiber weft of ECD450 yarns. One of these was called the standard pitch, and the interval of the weft pitch L_{wp} was 5.0 mm. The other was called the long pitch, and the interval of the weft pitch L_{wp} was 8.3 mm. The quasi-UD carbon fabrics were stacked as a quasi-isotropic lay-up: $[45/0/-45/90]_{2S}$. Then, they were cured with epoxy resin (DENATOOL XNR/H 6809, Nagase ChemteX Corp.) via a vacuum-assisted resin transfer molding (VARTM) process. The material properties of this UD composite are listed in Table 1.

Two kinds of composite laminates were fabricated from the aforementioned carbon fabrics using the VARTM method. To distinguish these laminates, we called the laminate fabricated with the standard pitch laminate I and the laminate fabricated with the long pitch laminate II. The fiber waviness of a composite laminate related to the quasi-UD carbon fabrics was characterized to analyze its effect on the compressive strength. A three-step method based on an FFT was used to obtain the characteristic wavelengths L_c and amplitudes A of the fiber waviness in the laminates.[9] A brief introduction of this three-step method is given below, and more details can be found in a previous study.[9]

a. Photographing a transverse cross section of the laminate in the length direction
Several photographs of a transverse cross section of the laminate were taken in the lengthwise direction and combined into a montage in the software Microsoft ICE, as shown in Figure 2(a). The

Table 1. Properties of this unidirectional carbon/ epoxy composite.[9]

Properties	Value	Properties	Value
Longitudinal modulus, E_{11}	160 GPa	Longitudinal tensile strength, X_t	2500 MPa
Transverse modulus, E_{22}	10 GPa	Longitudinal compressive strength, X_c	1300 MPa
Tangential modulus, G_{12}	5 GPa	Transverse tensile strength, Y_t	50 MPa
Major Poisson's ratio, ν_{12}	0.32	Transverse compressive strength, Y_c	150 MPa
Ply thickness, t	0.3 mm	Shear strength, S	100 MPa

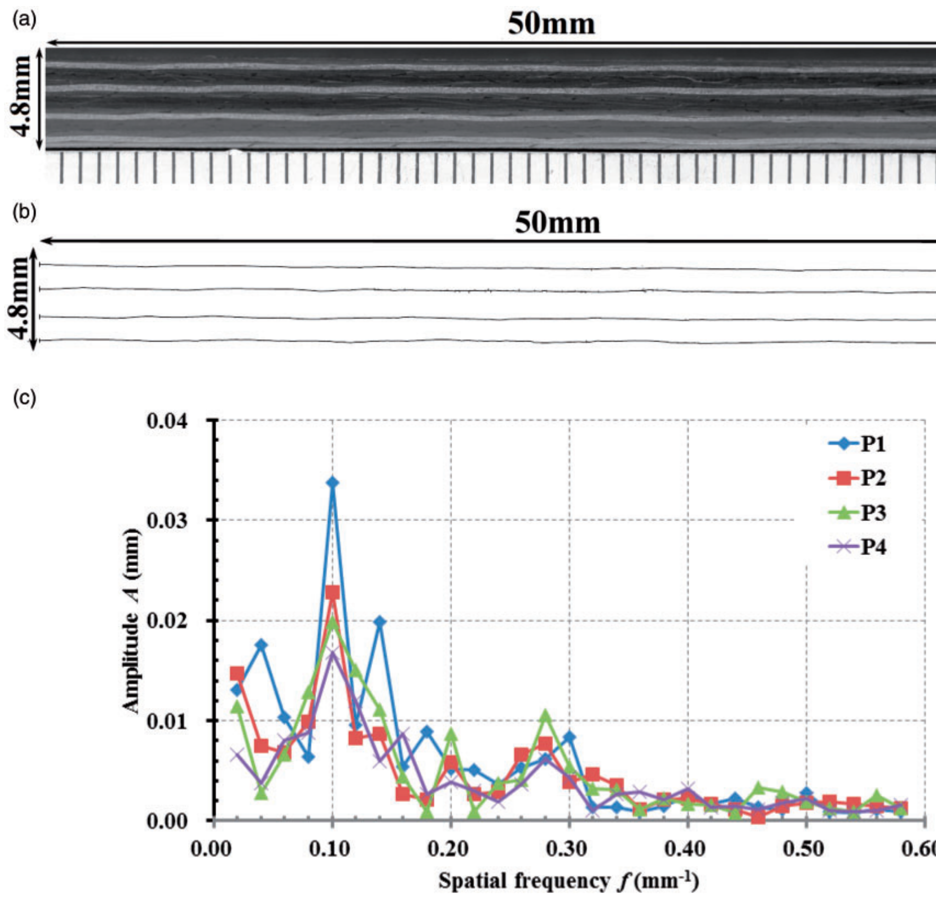

Figure 2. Three-step method for characterizing fiber waviness. (a) photographing transverse cross section, (b) thinning process for 0° layers, and (c) data processing.

stacking sequence of the laminate was [45/0/−45/90]$_{2S}$, as mentioned above, and the light layers labeled "P1," "P2," "P3," and "P4" in the figure correspond to the 0° layers.

b. Thinning process for 0° layers
The fiber waviness of each 0° layer shown in Figure 2(a) was treated as lines via the thinning process in the software CANVAS. The treated lines are shown as Figure 2(b). The pixel coordinates of each line were output for the next step.

c. Data processing based on the FFT
The pixel coordinates of each line were input to EXCEL, and the slope of the laminate to the camera was corrected. Afterward, a Fortran program based on the FFT was utilized to analyze the treated pixel coordinates. The spatial frequencies f and amplitudes A of each 0° layer were finally obtained, as shown in Figure 2(c), and the wavelength L_c of the fiber waviness was calculated using equation (4)

$$L_c = \frac{1}{f} \tag{4}$$

Three transverse sections from laminate I and four sections from laminate II were measured using the

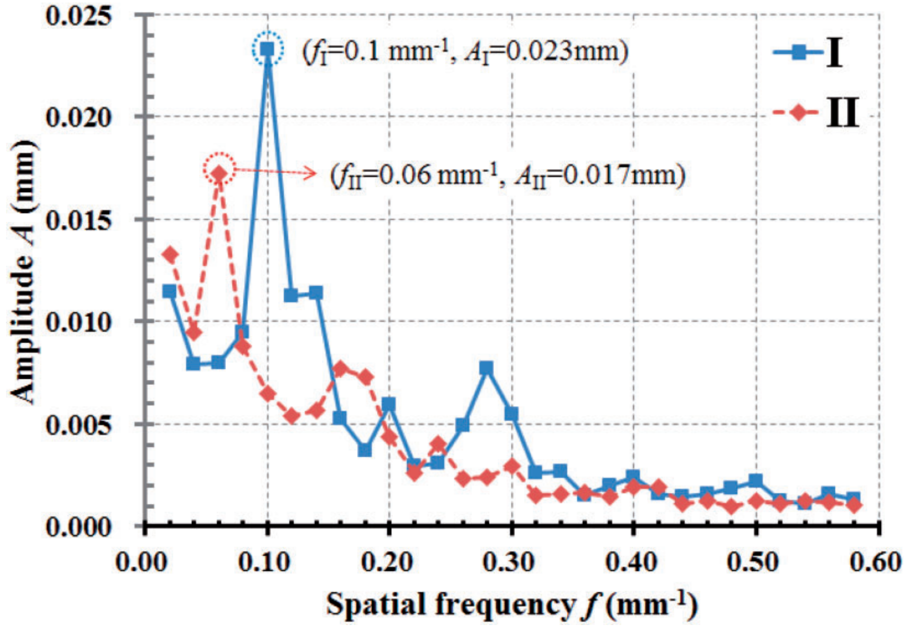

Figure 3. Relationships between average amplitudes and spatial frequencies in laminates I and II.

three-step method, and relationships between the average amplitudes and spatial frequencies in laminates I and II were obtained, as shown in Figure 3. The characteristic wavelength L_{cI} and average amplitude A_I of the fiber waviness in laminate I were 10.0 mm and 0.023 mm, respectively, with values of 16.7 mm for L_{cII} and 0.017 mm for A_{II} in laminate II. These results indicated that the characteristic wavelength of the fiber waviness L_c in the composite laminate was equal to double the interval of the weft pitch L_{wp}, as shown in equation 5. It also showed that the characteristic wavelength L_c of the laminate depended on the weft pitch interval of the carbon fabric.

$$L_c = 2L_{wp} \tag{5}$$

Experimental tests and results

Four specimens of each kind of laminate were used for the compressive tests, and each specimen was 135 mm long, 25 mm wide, and approximately 4.8 mm thick, which was shown in Figure 4(a). According to a predicted bucking stress based on simply supported end boundary conditions (equation 6), a central gage length of 35 mm was selected for a long gage area besides preventing a global bucking of the specimen

$$\sigma_{cr} = \frac{\pi^2 D_{11}}{h l_{ga}^2} \tag{6}$$

where D_{11} is an element of bending stiffness of the specimen, h is the total thickness, l_{ga} is gage length, and σ_{cr} is global buckling stress. Using the material properties in the Table 1, we calculated the global buckling stress with the gage length of 35 mm, which is 1183 MPa. This global buckling stress is twice as much as an expected compressive strength of the specimen. Furthermore, boundary conditions in the fixture are similar to the two ends fixed, which require a higher global buckling stress than that calculated from equation (6). Therefore, the global buckling will not happen before the compressive failure of the specimen.

Moreover, eight uniaxial strain gages were attached to each specimen to check out-of-plane and in-plane bending: strain gages 1 to 4 were on the front face of the specimen, and strain gages 5 to 8 were back-to-back gages mounted on the back face to correspond to the strain gages 1 to 4. The back-to-back biaxial 0/90° strain gages were attached to calculate the in-plane compressive Poisson's ratio.

A specimen was mounted in a support fixture as shown in Figure 4(b) and (c), which was built based on Shimokawa et al.'s study.[10] In this support fixture, each end of the specimen was fixed in place using 50-mm long binding grips. Considering the thickness of the specimen, some steel blocks with different thickness were selected and combined to keep the specimen on the centerline of the fixture, and eight screws were to clamp the specimen tightly. Although the fixture does not have any anti-buckling jig as described in ASTM D695, a pair of supporting guide and the steel blocks in the fixture prevent an out-of-plane movement of the specimen, and the strain gages are able to check whether the out-of-plane

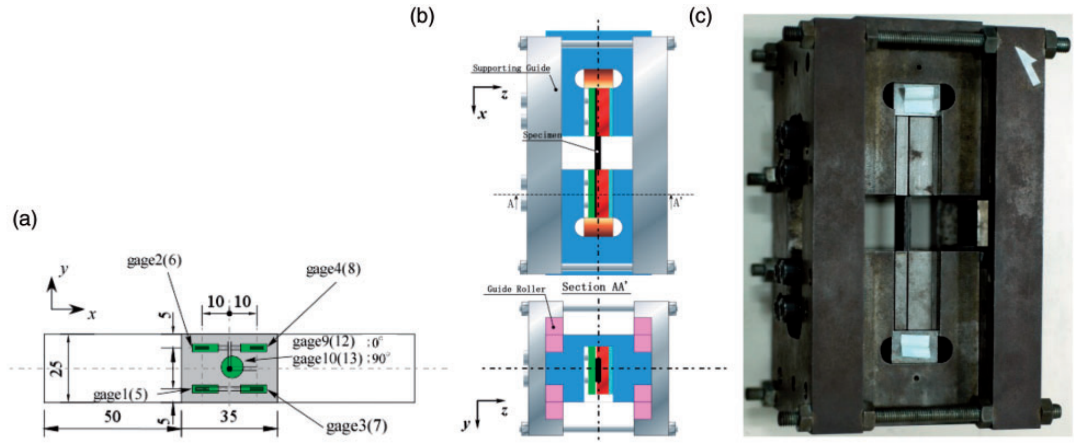

Figure 4. Compressive testing fixture: (a) specimen size, (b) schematic representation of fixture and specimen, and (c) photograph of fixture and specimen.

deflection occurred.[11] Then, the specimen/support fixture combination was installed in the testing machine (INSTRON 8501, ± 100 kN) for the compressive tests, and a compressive load was applied from end-sections of the specimen. An alignment test was preformed first to make in-plane and out-of-plane percent bending less than 10%, after that, the compressive test was conducted at a speed of 0.05 mm/min. The compressive load was immediately released upon the observation of any instability, which ensured the minimum post-failure damage was to the specimen. Finally, an assessment of the specimen stability was able to be provided from strain measurements to determine the occurrence of the global buckling in the specimen.

The experimental compressive strength was normalized to 60% fiber volume fraction because of the fiber volume fraction disparity between the different specimens, and these strength values are listed in Table 2. The average compressive strength of laminate I was 464 MPa, and that of laminate II was 481 MPa. This suggested that laminate II, which was fabricated with a long pitch, had a greater compressive strength than that fabricated with the standard pitch. A typical post-failure image was taken for each kind of laminate after the experiment; these images are shown in Figure 5.

Figure 5(a) shows a kind of brooming failure mode for laminate I.[12] The failure zone is in the 35-mm long gage section between two clamping lines of the fixture, and the height of failure zone after test is 13 mm, which is much bigger than initial thickness. According to the strain data from the strain gages in the gage section, the calculated maximum percent bending was about 5%, which indicates there was no onset of the global buckling in the tests. The 0° layers, marked as P1 to P4, are fractured, and the inner layers of laminate I are crushed and have a tendency to being extruded. Some delaminations occur among interfaces between the 0° layers and their neighborhood layers. Kelly and Hallstrom[13] demonstrated this failure mode, which was caused by laminate expansion, and an intralaminar and interlaminar fracture of the plies, which was promoted by the tensile through-thickness stress due to the expansion. In contrast, the post failure zone of laminate II shown in Figure 5(b) was slimmer than that of laminate I. In addition, the major damage occurs in the outer layers of laminate II, and a Z-shaped crack propagated through the inner layers. Same as the laminate I, the failure area of laminate II also occurs in the gage section of the specimens, and the global buckling did not happen because the percent bending was less than 10% in the tests. To explain the compressive strength and failure mechanism of laminates I and II, a numerical analysis is discussed in the next section.

Numerical analysis and discussion

The great advances in the calculation capacity of computers have made the finite element method (FEM) a powerful tool for understanding the failure mechanism using numerical calculations. In previous studies, models such as the wavy fiber unit cell model and wavy material-orientation model were proposed by Garnich and Karami[14–16] for UD composites. In this case, the lack of through-thickness stresses made it difficult to employ a 2D shell model based on the plane stress in the x-y plane. Therefore, a 2D plane mode based on the generalized plane strain was applied in the x-z plane, and two additional preconditions were employed, as listed below:

1. A new material was set as a counterpart of the 45° and −45° layers in the generalized plane strain model. The coefficients of mutual influence

Table 2. Comparison of compressive strengths.

	Compressive strength F_c (MPa)		Compressive strength F_c (MPa)
I-01	461.95	II-01	502.50
I-02	456.00	II-02	473.74
I-03	475.72	II-03	466.55
I-04	460.44	II-04[a]	429.15
I-Average	463.53	II-Average	480.93
S.D.	7.37	S.D.	15.53
C.V.	1.59%	C.V.	3.23%

[a]II-04 was neglected because of an unacceptable failure mode.

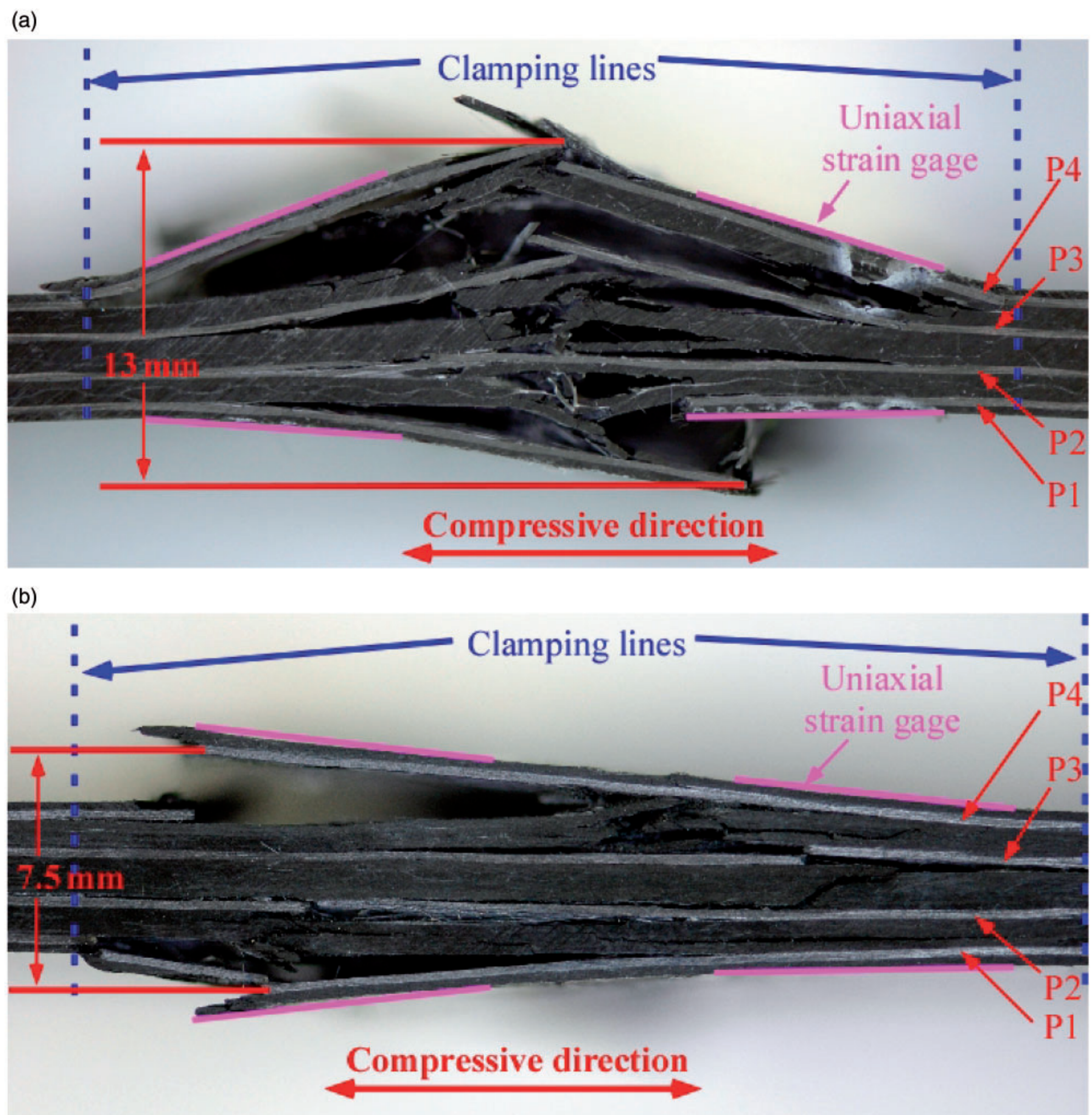

Figure 5. Images of typical post failure mode. (a) laminate I fabricated with standard pitch and (b) laminate II fabricated with long pitch.

corresponding to $\bar{Q}_{16}$ and $\bar{Q}_{26}$ of the 45° and –45° layers could not be input in this 2D model,[17] which affected the engineering constants in these two kinds of layers, such as by decreasing their modules E_x. Therefore, we averaged the elastic stiffness matrix $[C]$ of the 45° and $-45°$ layers using equation (7) and calculated the engineering constants using equation (8),[18] where the value of "•" depended on the angle of the layer. Finally, the lost stress τ_{xy} in this model could be obtained from equation (9)

$$[C]_{\overline{45}} = \frac{1}{2}[C]_{45} + \frac{1}{2}[C]_{-45} \tag{7}$$

$$[S]_\theta = [C]_\theta^{-1} = \begin{bmatrix} \frac{1}{E_{x\theta}} & \frac{-\nu_{xy\theta}}{E_{x\theta}} & \frac{-\nu_{xz\theta}}{E_{x\theta}} & 0 & 0 & \bullet \\ \frac{-\nu_{xy\theta}}{E_{x\theta}} & \frac{1}{E_{y\theta}} & \frac{-\nu_{yz\theta}}{E_{y\theta}} & 0 & 0 & \bullet \\ \frac{-\nu_{xz\theta}}{E_{x\theta}} & \frac{-\nu_{yz\theta}}{E_{y\theta}} & \frac{1}{E_z} & 0 & 0 & \bullet \\ 0 & 0 & 0 & \frac{1}{G_{yz\theta}} & \bullet & 0 \\ 0 & 0 & 0 & \bullet & \frac{1}{G_{xz\theta}} & 0 \\ \bullet & \bullet & \bullet & 0 & 0 & \frac{1}{G_{xy\theta}} \end{bmatrix}_\theta \tag{8}$$

$$\tau_{xy} = \overline{Q}_{16}\varepsilon_x + \overline{Q}_{26}\varepsilon_y \tag{9}$$

2. The calculated results in the x-z plane has to be translated into the material coordinate system using equation (10),[15] and the Tsai–Wu failure factor F_{tw} shown in equation (11) was used to determine whether or not an element failed.[16] The material properties of the failure elements decreased to 1% if F_{tw} was greater than one. In addition, we assume that the strengths of the composite in the z direction are the same as those in the y direction. In addition, the values of C_{12}, C_{23}, and C_{13} are simply set equal to zero, based on the results of Narayanaswami and Adelman[19]

$$\begin{bmatrix} \sigma_{11} \\ \sigma_{22} \\ \sigma_{33} \\ \sigma_{23} \\ \sigma_{13} \\ \sigma_{12} \end{bmatrix}_k = T_{\sigma k} \begin{bmatrix} \sigma_x \\ \sigma_y \\ \sigma_z \\ \sigma_{yz} \\ \sigma_{xz} \\ \sigma_{xy} \end{bmatrix}_k = \begin{bmatrix} m^2 & n^2 & 0 & 0 & 0 & 2mn \\ n^2 & m^2 & 0 & 0 & 0 & -2mn \\ 0 & 0 & 1 & 0 & 0 & 0 \\ 0 & 0 & 0 & m & -n & 0 \\ 0 & 0 & 0 & n & m & 0 \\ -mn & mn & 0 & 0 & 0 & (m^2-n^2) \end{bmatrix}_k \begin{bmatrix} \sigma_x \\ \sigma_y \\ \sigma_z \\ \sigma_{yz} \\ \sigma_{xz} \\ \sigma_{xy} \end{bmatrix}_k \tag{10}$$

where $m = \cos\theta$, $n = \sin\theta$, and T_σ is the transformation matrix of the stress

$$\begin{aligned} C_1 &= \frac{\sigma_{11}^2}{X_t X_c} + \frac{\sigma_{22}^2}{Y_t Y_c} + \frac{\sigma_{33}^2}{Z_t Z_c} + \frac{\sigma_{12}^2}{S^2} + \frac{\sigma_{13}^2}{S^2} \\ &\quad + \frac{C_{12}\sigma_{11}\sigma_{22}}{(X_t X_c Y_t Y_c)^{1/2}} + \frac{C_{23}\sigma_{22}\sigma_{33}}{(Y_t Y_c Z_t Z_c)^{1/2}} \\ &\quad + \frac{C_{13}\sigma_{33}\sigma_{11}}{(Z_t Z_c X_t X_c)^{1/2}} \\ C_2 &= \left(\tfrac{1}{X_t} - \tfrac{1}{X_c}\right)\sigma_{11} + \left(\tfrac{1}{Y_t} - \tfrac{1}{Y_c}\right)\sigma_{22} + \left(\tfrac{1}{Z_t} - \tfrac{1}{Z_c}\right)\sigma_{33} \\ F_{tw} &= C_1 + C_2 \end{aligned} \tag{11}$$

Based on the numerical method presented above, two unit models (M1 and M2) corresponding to single wavelengths of laminates I and II were built, respectively. The thicknesses h of the models M1 and M2 were equal to 4.8 mm, and the lengths of the models L_c were 10 mm and 17 mm, respectively. A curvature was introduced as the fiber waviness of each model in the length direction, as shown in equation (12), where the amplitudes of this waviness were 0.023 mm and 0.017 mm, respectively

$$W(x) = A[1 - \cos(2\pi x L)] \tag{12}$$

where A is the amplitude and L is equal to the wavelength.

For boundary conditions, which are also shown in Figure 6, the middle node at the left end of the model was fixed, and the other nodes at the left end were fixed in the length direction and free in the thickness direction. At the right end of the model, a displacement loading along the negative length direction was applied to all the nodes in this compressive calculation. In addition, the middle node at the right end of the model was fixed in the thickness direction, but the other nodes were free.

The compressive strengths from the simulations are 482 MPa for laminate I and 491 MPa for laminate II, respectively. We found that laminate II consistently had a greater compressive strength than laminate I, although this difference of the compressive strengths

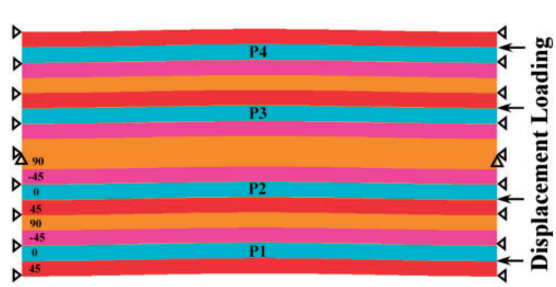

Figure 6. Boundary conditions for simulation.

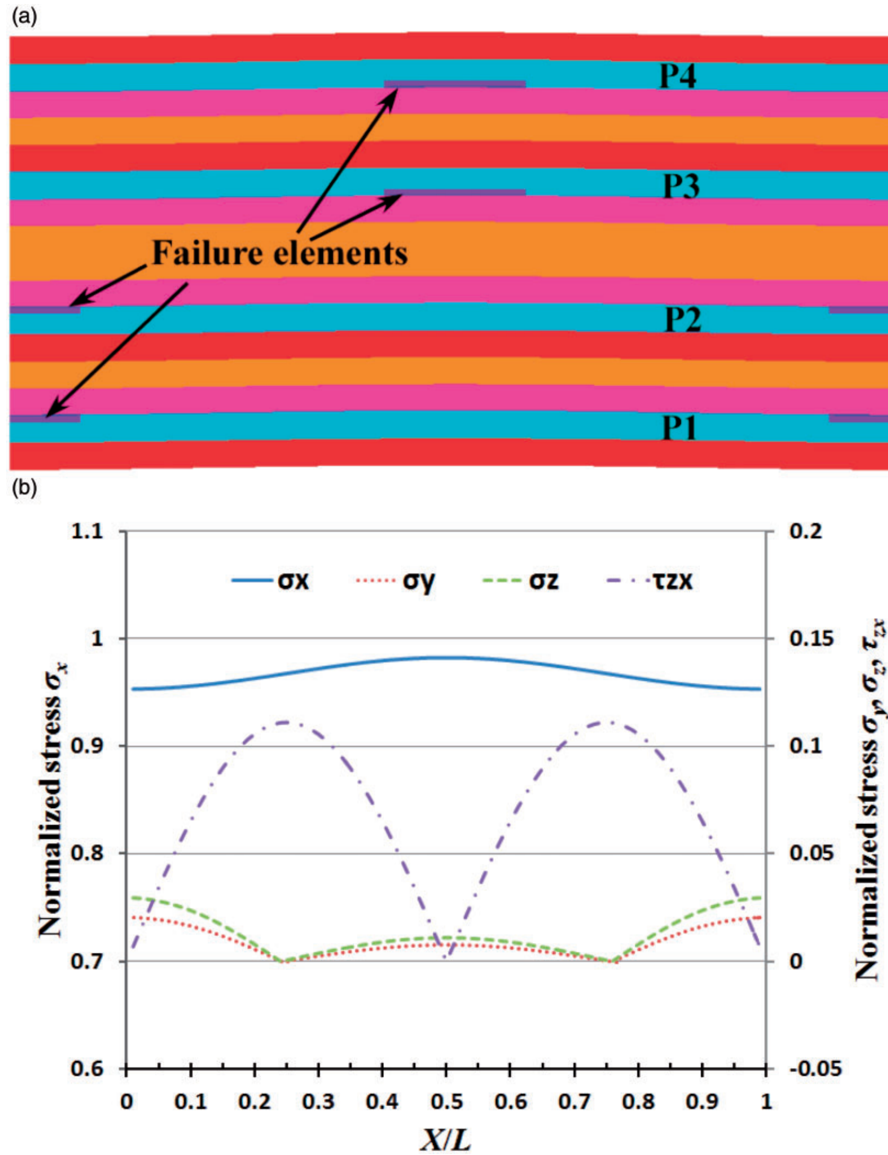

Figure 7. Failure mechanism in laminate I. (a) initial failure, (b) normalized stresses.

between laminates I and II from the simulations was not so obvious as that from the experiments. The reason was that the characteristic wavelength and averaged amplitude were used for simulation, but those were random in the laminates. Moreover, there were different failure mechanisms for laminates I and II, as shown in Figures 7 and 8.

In model M1, which corresponded to laminate I, the initial failure elements were found at the ends of layers P1 and P2 and in the middle of layers P3 and P4, as shown in Figure 7(a). The stress distributions of layers P1 at occurrence of initial failure were output and normalized to the corresponding strength, as shown in Figure 7(b), these normalized stress distributions evidenced the compressive stress σ_x and tensile through-thickness stress σ_z dominated this failure mode. Thus, we considered this failure mode to be the normal failure mode. However, the initial damage zone occurred at the middle of layer P1 and the ends of layer P4 in laminate II, as shown in Figure 8(a). The occurrence of the initial failure elements in layer P1 was strongly influenced by the compressive stress in the length direction σ_x due to bending, as shown in Figure 8(b). Therefore, the dominant failure mode in laminate II was the bending compressive failure mode, and it was also the reason why the post-failure zone of laminate II was slimmer in the experiments.

We also recognize that the shear stress τ_{zx} is an important value in the numerical analysis, which raised the fundamental question of whether a shear failure mode dominated by compressive-shear stress occurs when the amplitude of the fiber waviness A is great

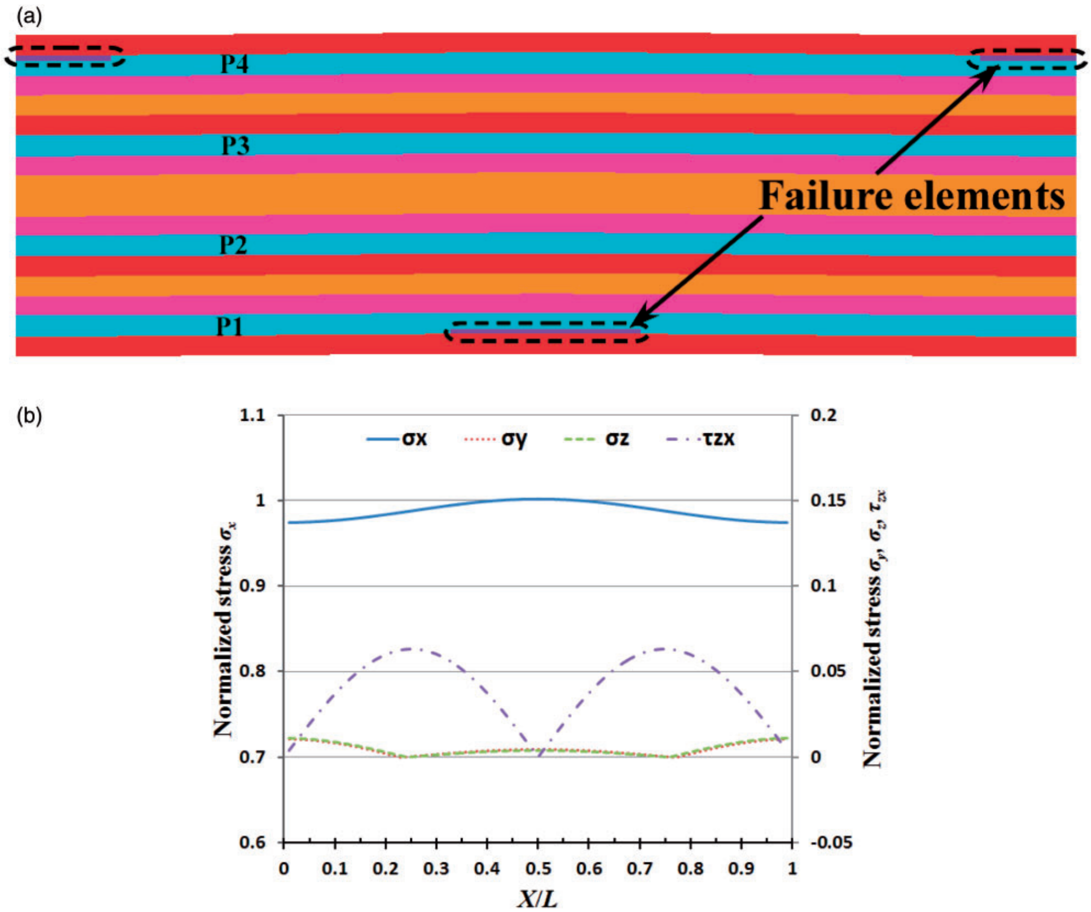

Figure 8. Failure mechanism in laminate II. (a) initial failure, (b) normalized stresses.

enough. Therefore, a parametrical study was conducted to investigate the shear failure mode, as reported in the next section.

Parametrical analysis

In order to investigate the shear failure mode, eight models with different wavelengths were created, and then five different amplitude-to-wavelength ratios A/L were introduced into each model. The wavelengths of the models ranged from 6 mm to 28 mm, and the maximum ratio was equivalent to 0.01 in each model. The compressive strengths were normalized based on the maximum compressive strength (498 MPa) from FEM calculations with A/L equal to zero, and are shown in Figure 9. Four regions with distinct failure mechanisms were found: region C was an axial compressive failure mode; regions N and B corresponded to the normal failure mode and bending failure mode discussed above, respectively; and region S was the shear failure mode.

The normalized compressive strengths showed a complex tendency because of the different failure mechanisms shown in Figure 9. In region N, the compressive strengths increased with decreasing ratio and increasing wavelength. This was because the tensile through-thickness stress decreased quickly at the same compressive stress when the wavelength was long with a small curvature. When the wavelengths increased with a smaller ratio, 0.0025, the model failed by slight bending in region B. Therefore, the normalized compressive stress decreased with an increase in the wavelength. Meanwhile, if the ratio increased, the shear stress increased and dominated the failure mode, with compressive stress in region S. Thus, the laminate damage was from the shear failure mode. Similarly, the compressive strength decreased with increasing wavelength because of the bending deformation, with the exception of a point whose wavelength was 8 mm at an A/L value equal to 0.01. This could be explained by the fact that the initial failure elements failed in the zone of tensile through-thickness stress at that point, whereas the other points in region S failed in the zone of compressive through-thickness stress. Moreover, the maximum strength could be observed near the boundaries between regions N and B or S for a fixed ratio, which implied that a good wavelength design for carbon fabrics could improve the compressive

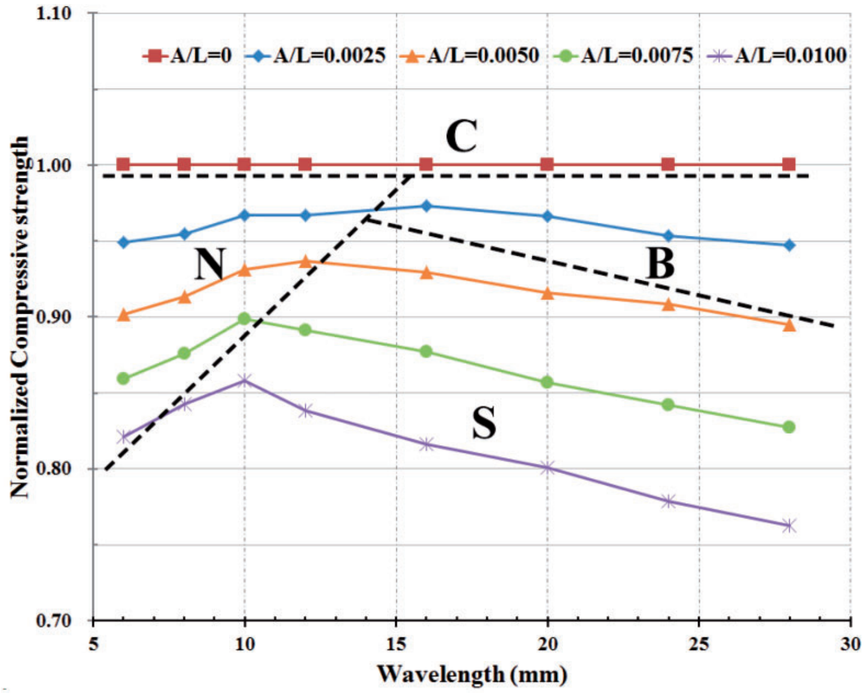

Figure 9. Normalized compressive strengths from parametrical study on ratios.

strength of laminates if the amplitude-to-wavelength ratio was known.

Conclusions

The effect of configuration of quasi-UD woven fabric on the compressive failure modes of quasi-isotropic composite laminates was studied in this paper. Compressive experiments were conducted first, and it was shown that the compressive strength of composite laminates fabricated with long-pitch weft fabrics was higher than that fabricated with standard-pitch weft fabrics. Then, numerical analyses were performed and the results were compared with the strengths from the experiments to obtain the different failure mechanisms for these two kinds of laminates.

A parameter investigation was conducted to analyze the effects of the wavelength of the fiber waviness and the amplitude-to-wavelength ratio, and four failure modes were mapped. This suggested that the configuration of the fiber waviness had a strong effect on the compressive strength of the quasi-isotropic composite laminates, and an optimized design for the configuration of the fiber waviness in a carbon fabric could improve the compressive strength.

Funding

This research received no specific grant from any funding agency in the public, commercial, or not-for-profit sectors.

Conflict of interest

None declared.

Acknowledgements

Wang is sponsored by the China Scholarship Council as a doctoral candidate at Kyushu University (File No. 201206290040). The authors also acknowledge Mitsubishi Rayon Co., Ltd. and Nagase ChemteX Corp. for providing the materials used in the experiments.

References

1. Rosen BW. *Mechanics of composite strengthening*. *Fiber Composite Materials*. Metals Park, OH: American Society of Metals Seminar, 1965.
2. Slaughter WS and Fleck NA. Microbuckling of fiber composites with random initial fiber waviness. *J Mech Phys Solids* 1994; 42: 1743–1766.
3. Argon AS. Fracture of composites. In: Herman H (ed.) *Treatise on materials science and technology*. New York, NY: Academic Press, 1972, pp.79–114.
4. Budiansky B. Micromechanics. *Comput Struct* 1983; 16: 3–12.
5. Shuart MJ. Failure of compression-loaded multidirectional composite laminates. *AIAA J* 1989; 27: 1274–1279.
6. Hsiao HM, Wooh SC and Daniel IU. Fabrication methods for unidirectional and crossply composites with fiber waviness. *J Adv Mater* 1995; 26: 19–26.
7. Hsiao HM and Daniel IM. Elastic properties of composites with fiber waviness. *Compos Part A-Appl S* 1996; 27: 931–941.

8. Hsiao HM and Daniel IM. Effect of fiber waviness on stiffness and strength reduction of unidirectional composites under compressive loading. *Compos Sci Technol* 1996; 56: 581–593.
9. Matsunoshita M. *Molding initial imperfections and compression-after-impact properties of VaRTM composites*. Master's Thesis, Kyushu University, Japan, 2010.
10. Shimokawa T, Hamaguchi Y, Kakuta Y, et al. Effect of isothermal aging on ultimate strength of high-temperature composite materials for SST structures. *J Compos Mater* 1999; 33: 1104–1118.
11. Uda N, Ono K and Kunoo K. Compression fatigue failure of CFRP laminates with impact damage. *Compos Sci Technol* 2009; 69: 2308–2314.
12. Odom E and Adams D. Failure modes of unidirectional carbon/epoxy composite compression specimens. *Composites* 1990; 21: 289–296.
13. Kelly G and Hallstrom S. Bearing strength of carbon fibre/epoxy laminates: effects of bolt-hole clearance. *Compos Part B-Eng* 2004; 35: 331–343.
14. Garnich MR and Karami G. Finite element micromechanics for stiffness and strength of wavy fiber composites. *J Compos Mater* 2004; 38: 273–292.
15. Karami G and Garnich M. Effective moduli and failure considerations for composites with periodic fiber waviness. *Compos Struct* 2005; 67: 461–475.
16. Garnich MR and Karami G. Localized fiber waviness and implications for failure in unidirectional composites. *J Compos Mater* 2005; 39: 1225–1245.
17. Whitney JM. Theory of an anisotropic elastic continuum. In: Whitney JM (ed.) *Structural analysis of laminated anisotropic plates*. Lancaster, Pa: Technomic Pub., 1987, pp.1–15.
18. Tsai SW and Hahn HT. Off-axis stiffness of unidirectional composites. In: Tsai SW and Hahn HT (eds) *Introduction to composite materials*. Lancaster, Pa: Technomic Pub., 1980, pp.65–109.
19. Narayanaswami R and Adelman HM. Evaluation of tensor polynomial and Hoffman strength theories for composite-materials. *J Compos Mater* 1977; 11: 366–377.